ISSN 0915-633X

NATIONAL INSTITUTE FOR FUSION SCIENCE

Direct Energy Conversion for IEC Propulsions

H. Momota, G.H. Miley and J. Nadler

(Received - July 24, 2000)

NIFS-641 Aug. 2000

RESEARCH REPORT
NIFS Series

NAGOYA, JAPAN

DIRECT ENERGY CONVERSION FOR IEC FUSION FOR SPACE APPLICATIONS

Hiromu Momota, George H. Miley*, and Jon Nadler

Professor Emeritus, National Institute for Fusion Science, Toki, Gifu, Japan
*Fusion Studies Laboratory, 103 S. Goodwin Avenue, Urbana, IL 61801, USA

Abstract

The paper describes a concept of extracting fusion power from D-^{3}He fueled IEC devices. The fusion system consists of a series of fusion modules and direct energy converters at an end or at both ends. This system of multiple units is linear and is connected by a magnetic field. A pair of coils anti-parallel to the magnetic field yields a field-null domain at the center of each unit as required for IEC operation A stabilizing coil installed between the coil pairs eliminates the strong attractive force between the anti-parallel coils. Accessible regions for charged particle trajectories are essentially isolated from the coil structure. Thus, charged particles are directed along magnetic field lines to the direct energy converter without appreciable losses. A direct energy converter unit designed to be compatible to this unique system is also described. It basically consists of a separator and a traveling wave converter. A separator separates low energy ions and electrons from the 14.7-MeV fusion protons and then converts their energy into electricity. In the traveling wave direct energy converter, fusion protons are modulated to form proton bunches. It couples with a transmission line to couple AC power out. The overall conversion efficiency of this system, combined with D-^{3}He IEC cores, is estimated as high as 60%.

Key Words: Inertia Electrostatic Confinement, D-^{3}He Fusion, Fusion Propulsion, IEC Array, Direct Energy Conversion,

1. Introduction

Inertia Electrostatic Configuration (IEC) devices[1-3] offer the community an ideal candidate for deep space propulsion due to it's relatively small reactor mass and capability of burning advanced fuels such as D-^{3}He. Indeed, the IEC works without magnetic fields and requires minimum shielding. Indeed, the parasitic D-D reactions, at optimum plasma energies, constitute ~10% of the reactions and ~2% of the power produced. The fusion core of an IEC reactor is confined inside a negatively biased grid structure that resides inside a grounded vacuum vessel. Various ion and electron sources are external to the cathode structure. The electric field associated with the grid accelerates the ions toward the center, focusing them into a dense peak. A representative density in the core is roughly 50 times the ion density at the grid region. As a result total fusion reactions will be enhanced, since the fusion reaction rate is proportional to the square of the ion density. Indeed several prior IEC propulsion studies have confirmed the attractiveness of this approach. But one of the key issues requiring further study involves the method to extract the fusion energy released.

With $^3He(d, p)^4He$ reactions, the fusion protons carry eighty percent of the liberated fusion energy. The recovery of this energy with direct energy conversion is essential for space propulsion. A directed exhaust of protons is possible, but this approach suffers from a low thrust (but very high specific impulse). Thus, the present study focuses on conversion of the fusion energy to electricity, which can then be used for propulsion and also station keeping. In an IEC, the proton birth velocity distribution is essentially isotropic; thus for present purposes these protons must be redirected. The present study applies a peripheral magnetic field around the IEC so as to "divert" protons with undesired directions and channel them into a direct energy converter. In this research, a configuration is developed whereby the magnetic field encloses the IEC but is essentially cancelled in the fusion reactive region. This is the essential point since internal magnetic fields can adversely affect IEC operation. Use with multiple IEC units allow a high total proton flux and energy production, while achieving system redundancy, which is viewed as essential for space missions.

Conventional electrostatic methods for direct electrical generation involve plates held at a high potential. Unfortunately, this requires potentials well over ten MV, which introduces severe voltage holding problems. One of the authors (H.Momota) has proposed a method to avoid this problem by employing traveling wave direct energy converters (TWDEC) for use with D-^{3}He fusion protons[4]. Detailed numerical analyses and preliminary experiments on the direct energy system have been carried out in Japan [5-6], confirming the feasibility of this approach and suggesting overall conversion efficiencies as high as 70%. While this results in a lower efficiency than using a direct proton beam into a thruster for space propulsion, it does offer some important advantages. Most importantly, the leaking

unburned fusion fuel (including ^{3}He) can be contained in the vacuum chamber and recycled. Further, the IEC requires some recycled electric power, which is easily obtained by diverting a fraction of the TWDEC output. It should be noted that the total system including direct energy converters is installed inside a vacuum chamber, whereby unburned fuels can be recycled avoiding unwanted loss of expensive fuels. With this approach converted electric power can be utilized with efficient, "off the shelf" electric thrusters such as an ion diode or a hall thruster.

In the next section, we will start by introducing an "*Accessible Region*" which covers the region containing charged particle trajectories following birth in the IEC. The concept is identical to "*Störmer Region*" which was first introduced to describe the aurora region. Configurations considered here have a vanishing magnetic field at the IEC region, otherwise the accelerated ion beam suffers unwanted divergence. Therefore, the accessible region of zero canonical angular momentum has to include the IEC region and must be isolated from the chamber wall as well as from the coil structure, while being channeled to the adjoining module or direct energy converters. A simple configuration where a pair of coils is installed anti-parallel to a uniform magnetic field provides the desired vanishing magnetic field near the center. This accessible region is completely isolated from the chamber wall as well as the coils. However, a support structure is required due to the strong attractive force between the two coils. This structure is not completely isolated from bombardment and will result in a significant drain of charged particles from the plasma. However to reduce these losses the uniform magnetic channel is replaced with a corrugated one, eliminating the attractive force between the coils. Consequently, only small pipes for feeding coil currents and coolant flow are used at the coaxial position. The estimated proton bombardment loss of the support structure is less than 0.36%.

The series of IEC modules is connected through a magnetic expander to the direct energy converter, which will be introduced in the following section. The direct energy system consists of a separator, a modulator, and a decelerator. The separator separates leaking fuel ion components and electrons from the 14.7-MeV fusion protons and converts their energy into electricity. The separator consists of hex-pole magnetic field and collector plates. Because of the light mass of the electrons, their trajectories lie on a magnetic surface that is connected to an electron collector plate installed at the edge of the flux surface. Low energy ions are scattered stochastically due to the lack of magnetic invariants at the null-field region. The kinetic energy carried by low energy ions and electrons is converted to electricity at the respective biased collector plates. Detailed studies are still underway.

One of the hardest technological challenges is recovering the energy carried by the fusion protons. Their energy of 14.7-MeV is much higher than normally encountered in complex high voltage systems. The present design effectively represents a linear accelerator operating in reverse: The bunching of energetic protons excites an oscillating, AC signal on the coupled transmission line. The phase velocity of the transmission line is decreased along the beam path to provide synchronization to the decreasing velocity of the modulated protons. A fraction of the excited electric power is utilized to modulate the proton beam at an upper stream. Thus the mechanism of the traveling wave direct energy converter is self-exciting and can be as a series operation of traveling wave tubes. Preliminary experiments have been successfully carried out in Japan and numerical simulations have showed an overall conversion efficiency as high as 70%.

The final section of this paper is devoted to concluding discussions. Results will be summarized and issues left as future studies are pointed out.

2. Accessible Island in a Module

A collision-less charged particle in an axially symmetric magnetic field conserves its Hamiltonian H and the canonical angular momentum P_θ defined respectively as:

$$H \equiv \frac{M}{2}\left(v_r^2 + v_\theta^2 + v_z^2\right) + q\,\varphi(r,z) \qquad (1)$$

and

$$P_\theta \equiv Mrv_\theta + \frac{q}{2\pi}\psi(r,z) \qquad (2)$$

Therefore, the following inequality defines the real values of the velocity components:

$$H - \frac{1}{2Mr^2}\left(P_\theta - \frac{q}{2\pi}\psi(r,z)\right)^2 - q\,\varphi(r,z) \geq 0 \qquad (3)$$

The quantity $\psi(r,z)$ is the magnetic flux and $\varphi(r,z)$ is the scalar potential. Cylindrical coordinates are used with the z-axis along the axis of symmetry. Since a particle is restricted to be in the region where the inequality (3) is satisfied, the region defined by this inequality is called the "*Accessible Region*". In an IEC, any charged particles such as leaking unburned fuel ions, fusion products, and

electrons are initially located at the origin. Therefore the canonical angular momentum of charged particle in an IEC vanishes. Further, the scalar potential can be ignored at a point distant from IEC region. Thus for our case an accessible region of a particle can simply be represented as

$$|\psi(r,z)| \le \frac{2\pi}{q} r\sqrt{2M \cdot W} \qquad (4)$$

The quantity M is the mass and W is the energy of the particle. A representative accessible region yielded by a pair of coils installed anti-parallel to a uniform magnetic field is illustrated in Fig.1. Coil currents are chosen such

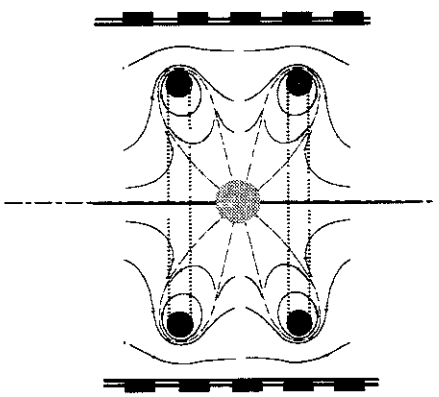

Fig.1: A pair of magnetic coils with fields anti-parallel to the uniform magnetic field yields an accessible region isolated from coils and vacuum wall. It also provides a field-null region near the center to allow installation of an IEC.

that the magnetic field at the center cancels out completely. One such favorable configuration employs "*Helmholtz Coils*", where spacing of the coils is equal to the coil radius R. This configuration provides a wide region with vanishing magnetic field. The coil current is chosen so as to eliminate magnetic field at the center. The resultant magnetic field is hex-pole combined with a magnetic field that is roughly proportional to $(r^2+z^2)^2/R^4$. The accessible region can be isolated from both the chamber wall and the coils if the applied coil current is sufficient. Nevertheless, an attractive force between the coils is typically 2 x 10^6N, if the coil current is 1-MAT and its major radius is 1m. A large fractional area of support structure in an accessible region spoils the favorable characteristics of the region. A corrugated magnetic channel is used to reduce or eliminate support structures.

Positioning the coils has to be done so in such a way that maximizes their stability. Then the canceling coils can be floated at their equilibrium position. Adjustment of the positional stability of a floating coil includes movement of the center of mass or rotation of it around the center of mass. The magnetic field that is measured by excluding the current on this coil is termed the "*External Magnetic Field*" while the magnetic field attributed to the current on this coil only is termed the "*Internal Magnetic Field*". Forces due to the internal magnetic field cancel out each another due to the equality law of action and reaction. Hence they do not contribute to a change in motion of the center of mass or to a rotation around it. The inner field acts only to deform the shape of the coil, which must be supported by the coils mechanical structure. Thus, the flux function and related magnetic field have to be studied on the basis of the external magnetic field $\bar{B}^{(e)}$ throughout the study of on positional stabilities.

A floating coil whose equilibrium position is at $z=Z$ is considered first. The coil has a major radius of R and a circular cross section of radius a. Positional modes include shifts perpendicular to the magnetic axis, shifts along the magnetic axis, and tilts. Those modes are illustrated in Fig.2. Assume the floating coil shifts along

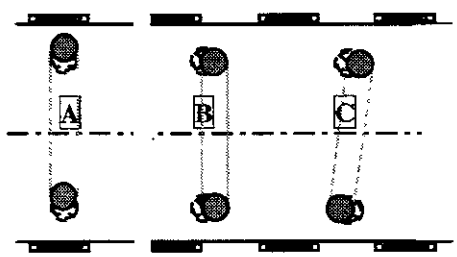

Fig.2: Illustrations of various positional modes: A, B, and C are a vertical shift mode, an axial shift mode, and a tilt mode, respectively.

the x-axis (perpendicular to the magnetic axis on the z-direction) by a small amount d_x from it's equilibrium position $x=0$. It then suffers an additional force is:

$$\delta F_x(R,Z;\delta_x) \equiv$$
$$\int J_\theta(r',z')\cos\theta \cdot B_z^{(e)}(\mathbf{r}'+\delta_x\cos\theta,z')\cdot r'd\theta dr'dz' \Rightarrow \qquad (5)$$
$$\frac{I_0}{a^2}\int_{z'=Z-a}^{z'=Z+a} dz' \int_{r'=R-\sqrt{a^2-(Z-z')^2}}^{r'=R+\sqrt{a^2-(Z-z')^2}} \frac{\partial B_z^{(e)}}{\partial r}(r',z')r'dr'\cdot\delta_x$$

The floating coil is therefore stable against shift modes perpendicular to the magnetic axis if the system satisfies the inequality

$$I_0 \cdot \frac{\delta < B_z^{(e)} >_a}{\delta r}(R,Z) < 0$$

$$\frac{\delta < B_z^{(e)} >_a}{\delta r}(R,Z) \equiv \frac{1}{\pi R a^2}\int_{z'=Z-a}^{z'=Z+a} dz' \int_{r'=R-\sqrt{a^2-(Z-z')^2}}^{r'=R+\sqrt{a^2-(Z-z')^2}} \frac{\partial B_z^{(e)}}{\partial r}(r',z')r'\,dr' \tag{6}$$

Stability of a floating coil against an axial displacement can be analyzed in a similar fashion. Assuming the floating coil shifts by an amount dz, the force on the floating coil in the direction of the z-axis can be expressed as

$$\delta F_z(r,z) \equiv -\int J_\theta \cdot B_r^{(e)}(r',z'+\delta_z)\cdot r' d\theta dr' dz' \Rightarrow$$

$$-\frac{2RI_0}{a^2}\int_{r'=R-a}^{r'=R+a} dr' \int_{z'=Z-\sqrt{a^2-(R-r')^2}}^{z'=Z+\sqrt{a^2-(R-r')^2}} dz' \frac{r'}{R} B_r^{(e)}(r',z') \tag{7}$$

$$-\frac{2RI_0}{a^2}\int_{r'=R-a}^{r'=R+a} \frac{r'}{R} dr' \int_{z'=Z-\sqrt{a^2-(R-r')^2}}^{z'=Z+\sqrt{a^2-(R-r')^2}} dz' \frac{\partial B_r^{(e)}}{\partial z}(r',z')\cdot \delta_z$$

The first term on the right hand side of this equation represents the force acting on the coil in the equilibrium position. Therefore, it should vanish:

$$< B_r^{(e)} > (R,Z) \equiv \frac{1}{\pi a^2}\int_{r'=R-a}^{r'=R+a} dr' \int_{z'=Z-\sqrt{a^2-(R-r')^2}}^{z'=Z+\sqrt{a^2-(R-r')^2}} dz' \frac{r'}{R} B_r^{(e)}(r',z') = 0 \tag{8}$$

Thus, the stability criteria is:

$$I_0 \cdot \frac{\delta < B_r^{(e)} >_a}{\delta z}(R,Z) > 0$$

$$\frac{\partial < B_r^{(e)} >_a}{\partial z}(R,Z) \equiv \frac{1}{\pi a^2}\int_{r'=R-a}^{r'=R+a} \frac{r'}{R} dr' \int_{z'=Z-\sqrt{a^2-(R-r')^2}}^{z'=Z+\sqrt{a^2-(R-r')^2}} dz' \frac{\partial B_r^{(e)}}{\partial z}(r',z') \tag{9}$$

Finally, we will discuss the stability condition of a floating coil against a tilt around the x-axis. The torque associated to the tilt angle d is

$$\delta T_x = -\int J_\theta B_r^{(e)}(r',z'+\delta\sin\theta)\; r'\sin\theta r' d\theta dr' dz'$$

$$\Rightarrow -\frac{I_0}{a^2}\int_{r'=R-a}^{r'=R+a} r'^2 dr' \int_{z'=Z-\sqrt{a^2-(R-r')^2}}^{z'=Z+\sqrt{a^2-(R-r')^2}} dz' \frac{\partial B_r^{(e)}}{\partial z}(r',z')\cdot\delta \tag{10}$$

Therefore, the floating coil is stable against tilt modes if

$$I_0 \cdot \frac{\delta < RB_r^{(e)} >_a}{R\delta z}(R,Z) > 0$$

$$\frac{\delta < RB_r^{(e)} >_a}{R\delta z} \equiv \frac{1}{\pi a^2}\int_{r'=R-a}^{r'=R+a} \frac{r'^2}{R^2} dr' \int_{z'=Z-\sqrt{a^2-(R-r')^2}}^{z'=Z+\sqrt{a^2-(R-r')^2}} dz' \frac{\partial B_r^{(e)}}{\partial z}(r',z') \tag{11}$$

is satisfied. If all the conditions (6), (9), and (11) are satisfied, the position of the coil is stable. It should be noted that quantities $\frac{\partial < B_z^{(e)} >_a}{\partial r}$ in (6), $\frac{\partial < B_r^{(e)} >_a}{\partial z}$ in (9), and $\frac{\partial < RB_r^{(e)} >_a}{R\partial r}$ in (11) tend to $\frac{\partial B_z^{(e)}}{\partial r}$, $\frac{\partial B_r^{(e)}}{\partial z}$, and $\frac{\partial B_r^{(e)}}{\partial z}$ respectively. Ampere's law, however, states that these quantities are identical in a vacuum:

$$(\mu_0 J_\theta(r,z) =) \frac{\partial B_r^{(e)}}{\partial z}(r,z) - \frac{\partial B_z^{(e)}}{\partial r}(r,z) = 0 \tag{12}$$

Therefore, a floating coil with zero cross section can't be stable. In the case of finite cross section of a floating coil, conditions (6), (9), and (11) can be made consistent. This is attributed to the fact that no external magnetic field near regions $r=R\pm a$ contributes to condition (6) for a perturbation d_x. However, this field does contribute near regions $z=Z\pm a$. For a perturbation d_x or d, however, the status is quite different. The external magnetic field near regions $(r=R\pm a)$ contribute greatly to the dynamics that do not lie near the region $z=Z\pm a$. Keeping this in mind, a stable configuration for a floating coil can be sought by installing carefully stabilizing coils.

Wholly stable configurations studied so far appear to intersect the accessible region. That gives appreciable amounts of unwanted particle or energy losses due to coil bombardment. Thus studies of these lines are left for the future. Consequently, condition (6) will be ignored for practical purpose. Thin pipes for feeding current or for recycling coolant to the coil can support the floating coils mechanically, if shift modes perpendicular to the magnetic axis are only weekly unstable. A possible configuration is illustrated in Fig.3, in which the stabilizing coil is installed at the center of two floating coils. Each floating coil with a major radius of 1.5 m curries 25 MAT. Detailed system parameters are listed in the Table 1. The accessible region created by a pair of floating coils and a stabilizing coil is isolated from both magnetic coils and chamber wall. The region between the

outer lines and circles around the floating coils is the accessible region for 14.7-MeV protons yielded through $^3He(d, p)^4He$ reactions. Lines from the center represent thin accessible regions of electrons. Due to additional

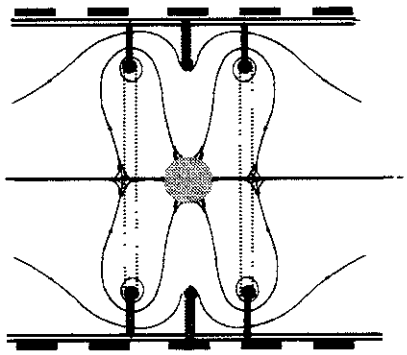

Fig.3: Accessible region by a pair of floating coils and a stabilizing coil is isolated from magnetic coils and vacuum wall. Region between outer lines and circles around floating coils is the accessible region for 14.7-MeV protons. Lines from the center are thin accessible region for electrons.

Table 1: Representative Parameters of the Coil System

Floating Coil (each of two)	
Major Radius: R_0	1. 5 m
Cross Section: pa^2	$\pi \times 0.075^2$ m^2
Current: I_0	-2. 25 MAT
Conductor	HeII cooled Nb_3SnO_4
Axial Position: Z_0	$\pm$ 0. 75 m
Stabilizing Coil	
Major Radius	$\pm$ 1. 5 m
Cross Section	$\pi \times 0.044^2$ m^2
Current	0. 7811 MAT
Conductor	HeII cooled Nb_3SnO_4
Axial Position	0 m
Solenoid	
Inner Radius	2. 1 m
Current/Length	0. 76213 MAT/m
Magnetic Field	0. 9577 T

coils, the area of null-magnetic field near the center decreases to a 75% of the original one. Nevertheless, within the sphere of a radius 0.32 m, the magnetic field is less than 1% of the original magnetic field; and inside the sphere of a radius of 0.09 m, the magnetic field is less than the 0.1% that is relevant for biased grid region of an IEC to obtain a favorable operation. Thus we are able to keep an area of vanishing magnetic field large enough to install an IEC by installing a bombard-less coil system.

The force balance of the floating coil is obtained, since the radial component of the averaged external magnetic field at the point $< B_r^{(e)} >$ defined by the equation (8) takes the value zero at the point *(R,Z)*.

Quantities $\frac{\delta < B_r^{(e)} >}{\delta z}_{(R,Z)}$ and $\frac{\delta < RB_r^{(e)} >}{R\delta z}_{(R,Z)}$

defined by equations (9) and (11) respectively, are obtained numerically to give the same value –0.181847 T/m. Since the coil current I_0 is negative, the system is stable against axial shift modes or tilt modes. The stability of vertical shift modes, is defined by a positive value of $\frac{\delta < B_z^{(e)} >}{\delta r}_{(R,Z)}$. This quantity takes a value of 0.181761T/m in our configuration. Thus, the system is unstable to these modes. It may possible to obtain a stable system against any modes by installing additional stabilizing coils. Those coils have to be installed close to the floating coil and consequently intersect the isolated accessible region. If the coil shifts vertically from its equilibrium position by a distance of only 0.001m, the resulting force acting on a floating coil is 3.85×10^3 N. Fortunately, 4 pipes connected to the coil, one for current feeding coaxial cable and other two for coolant recycling, are capable of supporting this force. Each pipe is made of conventional materials with a stress of 30 kg(w)/mm^2 and has 0.005m outer radius and 0.0005 m thickness. Bombardment loss of particles onto these pipes is estimated to be less than 0.36%. Thus in view of practical applications, it is best to neglect the instability of vertical modes at this time.

Fortunately, an area where the magnetic field is weak enough to operate an IEC of high efficiency exists in a magnetic channel suitable for direct energy conversion. The bombardment losses of particles on the coil structure are so small that modules can be analyzed, if necessary, in series along the magnetic channel, extending to a direct energy converter.

3. Direct Energy Conversion

With $^3He(d, p)^4He$ reactions, 14.7-MeV fusion protons carry eighty percent of the fusion energy released. The recovery of their energy with direct energy converters is essential for space propulsion. The energy is, however, much higher than the practical for use of a biased electrostatic electrode. Energy carried by leaking unburned fuel ions as well as electrons should be recovered also. All the equipments are installed inside a vacuum chamber; therefore, unburned fuel can be recovered and recycled after it is pumped out from the container. Recovered energy will be utilized to accelerate

unneeded ions up to an optimum momentum. One propulsion method assumes that energetic fusion ions and leaking unburned charged particles are converted directly to thrust. In this method, however, the momentum ejected per second through the thruster is fixed. Since the burning fraction of $^3He(d, p)^4He$ fusion may be less than several percent, the majority of the expensive fuels including helium-3 must be ionized and would be exhausted to the space without releasing fus' energy. While the present scheme avoids this waste b recycling fuel, the recovery of their energy with a dir.. energy converter is still essential.

Charged particles flowing out of fusion core include 14.7-MeV fusion protons as well as unburned fuel ions and others. These particles will be accelerated by an expanding magnetic channel and conducted to the separator. At the downstream of the expander, a magnetic separator is installed. The magnetic field attributed to the solenoid at the separator is 0.1198 T. Since magnetic field is 0.9577 T at the entrance of the expander, more than 87% in the total kinetic energy of charged particles is converted to the kinetic energy

Table 2: Representative Parameters of the Separator

Separator Coil (each of two)	
Major Radius	3. 0 m
Cross Section	0. 08m×0. 05m
Current	0. 2 MAT
Conductor	HeI cooled NbTi
Axial Position	1. 5 m
Solenoid	
Inner Radius	3. 2 m
Current/Length	0. 0953 MAT/m
Magnetic Field	0. 1198 T

parallel to the magnetic field during passage through the expander. The magnetic separator is formed at a region past the expander by installing a pair of coils anti-parallel to the axial field. Detailed parameters of the separator are listed in the Table 2. Pitch angles of electrons, leaking unburned fuel ions, and low energy fusion products such as ^{4}He are scattered randomly at the field- null region[7] and recombined at the surface of collector plates installed at the edge of respective accessible regions. An example of the magnetic separator is illustrated in Fig.4.

The region between outer solid lines and solid semi-circles around the coils in Fig. 4 is the accessible region for accelerated 200-keV deuterium ions. Dotted lines crossing the center are the thin accessible regions for electrons. Since the mass of electron is extremely small, they are conducted along the first line to the electron collector plate installed at the edge of their

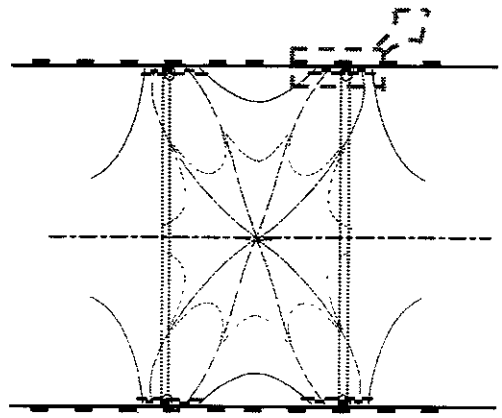

Fig. Fig.4. Magnetic configuration of the hex-pole separator: Electrons and leaking unburned fuel ions are conducted to the collector plates. 14.7 MeV fusion protons are passing through the separator attributed to their large inertia.

accessible region. Accelerated leaking unburned fuel ions are also trapped at the separator and conducted to ion collector plates at the edge of the region. Low energy fusion products such as ^{4}He are collected as well.

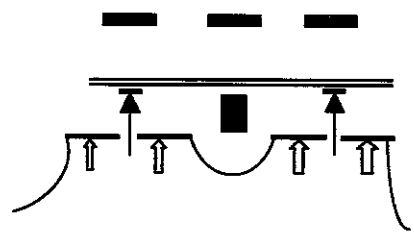

Fig.5. Installations of collector plates: Electrons are conducted to the electron collector plate through a thin accessible region, as is shown by the arrow. The accessible region of ions, on the other hand, extends out well past both sides of the electron stream. A majority of ions are therefore conducted to ion collector plates installed at the edge of ion accessible region in both sides of electron flows. Block arrows in the figure show ion flows, while the thin block arrows show electron flow.

Fig.5 shows the structure of a collector. Despite the simplicity of this system a conversion efficiency higher than 45% is obtained. The 14.7-MeV protons carry the majority of fusion power in D-^{3}He fusion system. Since the inertia of these protons is very high, they pass through the separator without suffering either trapping or an appreciable change in pitch-angle. The energy spectrum of fusion protons is exhibited in Fig.6.

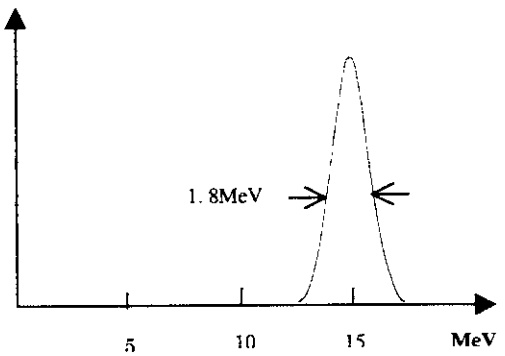

Fig.6. Energy distribution of $^3He(d, p)^4He$ produced protons. 94% in the total energy is carried as the free energy.

Their distribution function can be approximated by a shifted maxwellian distribution:

$$f(v)=\frac{n}{\sqrt{\pi}v_T}\exp[-(v-v_p)^2/v_T^2] \tag{13}$$

Where $v_p \equiv 5.307\times10^7$ *m/s* is the velocity of fusion protons. Due to the thermal spread of fuel ions in an exothermic reaction, fusion protons exhibit a thermal spread of 0.9 MeV. Nevertheless, 94% in the total energy is available for conversion. Using biased ion collector plates requires an electrostatic potential as high as 15 MV. This value exceeds the present technological capability limit. Therefore, to avoid this problem, a traveling oscillator is proposed to convert beam energy into electricity. Figure 7 shows an equivalent circuit of a converter.

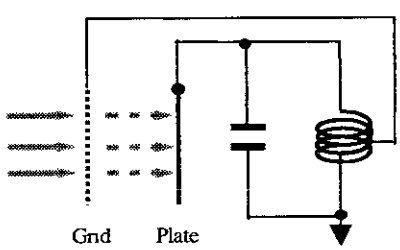

Fig.7: An equivalent circuit of beam-AC electricity converter. The applicable voltage is, however, too low to fully utilize beam energy of 14.7MeV protons.

The alternating electric voltage applied to the grid modulates the velocity of the charged particle flow. This modulated beam then results in an electro-motive force on the electrode plate. The electrode is connected to an LC resonance circuit while a fraction of the output AC voltage is fed back to the grid. By adjusting the phase a self-excited alternating electrical power is obtained. The maximum voltage applicable to the electrodes is, however, a few mega-volts in order to break the voltage down. This system seems most useful for a low-energy particle beam. For a 14.7-MeV fusion proton beam, however, only a few percent of the beam energy will be converted to electricity. However, replacing the electrode plates by grid meshes to form a series of electrodes provides a drastic upgrade of the system for use with the 14.7-MeV proton beam. The layout of the upgraded traveling wave direct energy converter is illustrated in Fig.8. At the modulator *(0,L)*, the fusion proton velocity flow is modulated by an applied alternating voltage:

$$V(z,t)=V_m\cos kz\cdot\sin\omega t \tag{14}$$

Consider the case where the applied voltage in the modulator is small and consequently changes in the velocity are a perturbation of the initial velocity of particles. Here wave number k stands for p/L. After passing through the modulator, the velocity of a particle that entered with a velocity v_0 at the time t_0 is changed to velocity v given by:

$$v=v_0-\frac{1}{4v_0^2}\frac{qV_m}{M}L\omega\cos\omega t_0 \tag{15}$$

Since the distribution function (13) is modified at the modulator and no oscillating electric field appears down stream, the distribution function at the time t and the position $z\,(>L)$ is expressed by:

$$f(z,v,t)=\frac{n}{\sqrt{\pi}v_T}\exp\left[-(v-v_p)^2/v_T^2\right]\times \times\left\{1+\frac{v-v_p}{v_T^2}\frac{L\omega}{2v^2}\frac{qV_m}{M}\cos(\omega t-\frac{\omega z}{v})\right\} \tag{16}$$

In order to examine the bunching, equation (16) is integrated to obtain the particle density of fusion protons:

$$n(z,t)=n\left[1+kz\frac{\pi qV_m}{Mv_p^2}\cdot\sin(kz-\omega t)\right] \tag{17}$$

for $z>L$

Equation (17) shows that the modulation of the number density of beam protons. In order to examine the bunching, equation (16) is integrated to obtain the particle density of fusion protons:

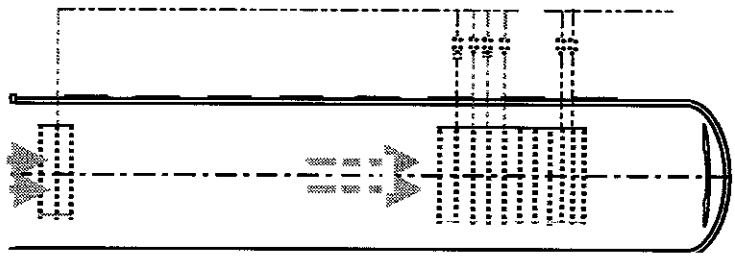

Fig.8. Traveling wave direct energy converter composed of an array of modulator grids upstream followed by an array of decelerator grids downstream. Each grid is connected to a transmission line. The modulator forms bunches of the charge, modulating the 14.7-MeV proton beam. Bunching the charge induces grid meshes an alternating electromotive force electromotive force.

$$n(z,t)=n\left[1+kz\frac{\pi qV_m}{Mv_p^2}\cdot\sin(kz-\omega t)\right] \qquad (17)$$

for $z > L$

Equation (17) shows that the modulation of the number density of fusion proton increases along the flow line. At a point near

$$z \approx Mv_p^2/k\,\pi qV_m \qquad (18)$$

bunching of the proton beam is completed, and an array of meshed grids is installed at this point. Once a meshed grid is located in the bunched beam region, it suffers from an induced electrostatic electromotive force through a space capacitance *Cs*. Each meshed grid is connected to a transmission line; therefore, the induced electromotive force excites an alternating AC signal

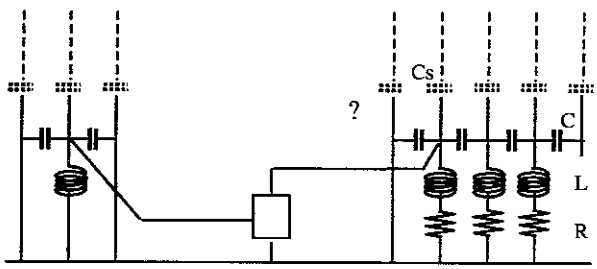

Fig.9: Transmission Line connected to an array of decelerator's. A part of voltage in the line is fed back to the modulator.

on the line. A part of the voltage is fed back to the modulator. The principle of circuit is illustrated in the diagram of Fig.9. The potential $V_n^b(t)$ of the bunching beam at the nth grid induces an electromotive force on the grid through the stray capacitance C_s between the beam and the grid. The potential $V_n(t)$ at the nth terminal (indicated by a symbol ? on the figure) is related to the capacitance *C*, connected to adjacent terminals with the inductance *L* and resistance *R* being connected in series to ground. The circuit equation for this system takes a form:

$$\left(2+\frac{C_s}{C}\right)\left(\ddot{V}_n+\frac{R}{L}\dot{V}_n\right)+\frac{V_n}{LC}-\left[\ddot{V}_{n+1}+\ddot{V}_{n-1}+\frac{R}{L}(\dot{V}_{n+1}+\dot{V}_{n-1})\right]=\frac{C_s}{C}\left(\ddot{V}_n^b+\frac{R}{L}\dot{V}_n^b\right) \qquad (19)$$

The derivation of this equation follows from applying Ohm's law and the equation of continuity for currents into and out of a terminal. Due to interactions with the grid potential, the bunching beam changes its velocity and the consequent potential of the beam $V^a(z,t)$ in the grid region takes a form $E_{z_n}^e \sin(\int k_d(z)dz-\omega t)$. The solution to equation (19) can be written in the form:

$$V_n(t)=f_p(t)\cdot\cos(\theta_n-\omega t) \qquad (20)$$

with a slowly varying amplitude. This assumes that the phase velocity of the transmission line is identical to the beam velocity. Then the equation (19) can be separated into two: one represents the high frequency part

$$\left(2(1-\cos\delta)+\frac{C_s}{C}-\frac{1}{\omega^2CL}\right)f_p(t)=E_{z_n}^e\frac{C_s}{\omega C}\sqrt{(R/L)^2+\omega^2}\times\sin\left(\int_{z_n}k(\xi)d\xi-\theta_n+\cos^{-1}\frac{R/L}{\sqrt{(R/L)^2+\omega^2}}\right) \qquad (21)$$

and for the slowly varying part

$$\left(2(1-\cos\delta)+\frac{C_s}{C}\right)\left(2\dot{f}_p(t)+\frac{R}{L}f_p(t)\right)$$
$$=E^e_{z_n}\frac{C_s}{C}\sqrt{(R/L)^2+\omega^2} \qquad (22)$$
$$\times\cos\left(\int_{z_n}k(\xi)d\xi-\theta_n+\cos^{-1}\frac{R/L}{\sqrt{(R/L)^2+\omega^2}}\right)$$

Here, we have introduced the quantity: $\delta\equiv\theta_{n+1}-\theta_n$ that is constant of n due to the same circuit constants at each terminal. Then, the quantity $V_{n+1}+V_{n-1}$ is expressed as $2V_n\cos\delta$. There are now two equations for the slowly varying amplitude. A non-trivial solution to equations (21) and (22) exists only if the dispersion equation:

$$2(1-\cos\delta)+\frac{C_s}{C}-\frac{1}{\omega^2CL}=0 \qquad (23)$$

is satisfied and the phase relation is presented. For a case of increasing solution, the phase relation is:

$$\int_{z_n}k(\xi)d\xi-\theta_n+\cos^{-1}\frac{R/L}{\sqrt{(R/L)^2+\omega^2}}=0 \qquad (24)$$

Then, the solution to the equation (19) is:

$$V_n(t)=E^e_{z_n}C_sQ[1-\exp(-Rt/2L)]\cos(\theta_n-\omega t) \qquad (25)$$

The quantity $Q\equiv\sqrt{\omega^2L^2+R^2}/R$ is the Q-value of the resonance. The solution (25) shows that an oscillation grows automatically by itself. Indeed, the solution takes a simpler form if the value $Rt/2L$ is much smaller than unity:

$$V_n(t)=E^e_{z_n}C_sQtR/2L \qquad (26)$$

For a large value of $Rt/2L$, however, the potential saturates at a certain level given by:

$$\left|V_n(t)\right|=E^e_{z_n}C_sQ \qquad (27)$$

Thus the amplitude of the excited oscillation on the transmission line is proportional to the electromotive force on a grid multiplied by the Q-value of the resonance, therefore, inversely proportional to the load resistance R that designates the load on the power output.

The base of this model is the condition that the beam velocity $v(t)$ is identical to the phase velocity of the transmission line $\omega/k_d(z)$. The equation of motion for bunching proton beam:

$$M\frac{d^2}{dt^2}z(t)=-qk(z)V^b\sin\left(\int k_d(z)dz-\omega t\right) \qquad (28)$$

gives the needed wave number for the transmission line to meet this requirement. Thus the spacing of meshed grids must be arranged to satisfy the condition:

$$k_d(z)=\frac{\omega}{v_p}\left(1-\frac{3qV^b\omega}{Mv_p^3}z\right)^{-1/3} \qquad (29)$$

In a decelerator, energy carried by bunching protons is converted to electricity on a transmission line by selecting the relative phase between bunched protons and the traveling wave at a relevant value. The physical process of this conversion is exactly the inverse of that is in a linear accelerator, which converts electric energy into a kinetic energy of the charged particles by choosing the relative phase between a traveling wave and charged particle to be an adequate value. The relative phase difference is inverse to that of the decelerator. In both processes, a reasonable value of relative phase provides the auto-phasing that appreciably improves the overall conversion efficiency. The relative phase is kept constant automatically and consequently the bunching of fusion protons is maintained.

Details of the grid mesh structure have been studied, as a part of a converter design for a 1-GW_e D-^{3}He fueled FRC power reactor[8,9]. Direct energy converters were installed at both ends of a field-reversed configuration. The radius of the grid arrays is 5m and averaged power flow at the entrance of the decelerator was approximately 10 MW/m^2. Each meshed grid is made of coaxial rings of water-cooled pipes. The spacing of pipes was typically 1.06 m. In order to decrease unwanted bombardment loss of fusion protons onto the grid structure, pipes with an outer diameter of 0.01 m are employed. Then the average transparency of protons was 98.8% for every passage of grid structure. Major characteristics of grid pipes are listed in Table 3.

Table 3: Major characteristics of Grid Pipes

Material: Stainless Steel
Cooling: Water Flow in the Pipe
Maximum Length: 10m
Outer Diameter: 0. 01m
Inner Diameter: 0. 009m
Water Pressure at the Inlet: 15MPa
Water Temperature at the Inlet: 20 °C
Flow Velocity: 10m/s

By applying a flow velocity of 10 m/s, a maximum flow

temperature of 200 ^{0}C and a maximum flow pressure of 15 MPa are obtained. These values are compared with the saturation temperature of water 335 ^{0}C and the limiting stress pressure of stainless steel of 42 MPa or that of copper 31 MPa. Meshed grid structures are immersed into a 14.7-MeV proton flow. After the separator, however, the flow density is as low as 4.25×10^{17} protons/m^{2}sec. Because of this low flux density and high bombarding energy, pipes are estimated to last more than 100 years against sputtering due to protons.

Numerical simulations of the traveling wave direct energy converter for the D-^{3}He fueled FRC power reactor have been carried out intensively in Japan. A fairly large flexibility is retained in determining the size of a traveling wave direct energy converter. Flashover voltage requires a certain spacing of the grid and peripheral technologies such as the high power rectifier sets a lower frequency. In order to limit the size of the converter to a reasonable value, the wavelength of the modulator was selected to be 6.28 m. Accordingly, the characteristic frequency of the system was 8.54 MHz, which frequency seems reliable to rectify for AC-DC or AC-DC-AC converters. Electrostatic potential due to a non-neutral proton bean in the TWDEC is a couple of hundred kilovolts and gives no contribution to the proton dynamics. Then automatic startup and saturation of the alternating power on the transmission line occurs in about 600 periods (70μs) after switching it on. The maximum conversion efficiency is obtained by choosing the voltage on the grid as 1.7 MV. This is accomplished by adjusting the load resistance or Q-value of the resonance circuit. The optimization with respect to the position of the decelerator shows that the entrance of the decelerator should be 10% beyond the point where the modulation takes its maximum. The obtained conversion efficiency is as large as 65 %, if the bombardment loss of fusion protons to the grid pipes can be neglected.

4. Conclusion and Discussion

A concept has been proposed to allow the extraction of fusion power from nearly aneutronic fusion fuels, such as D-^{3}He in an IEC, and to convert it into electricity.

An IEC fusion core is installed at the center of a pair of coils that cancels the uniform magnetic field providing channeling of ions into direct energy converters. To eliminate the strong attractive force between the coils, a stabilization coil is installed between the coils. Installation of the IEC requires a negligible magnetic field in the dense core region. With the present design, a spherical region at the center of a module is obtained with a radius of 6% of the canceling coil. This result is achieved when the magnetic field is less than 0.1% of the uniform magnetic field. Fusion charged particles are trapped within an accessible region, extending outside of the IEC but isolated from magnetic coils and the vacuum chamber. To minimize charged particle bombardment, the pipes for current feeding and for coolant recycling must have a high transparency perpendicular to the beam.

This configuration allows for operation of the IEC's in series along the magnetic channel. An IEC module, or a series of IEC modules, is connected to the direct energy converter through a magnetic expander, which changes the perpendicular component of kinetic energy of charged particles into the parallel component. The direct energy converter consists of a separator and a traveling wave direct energy converter. Low energy charged particles such as electrons, leaking unburned fuel ions, and fusion the fusion product, ^{4}He are separated from the 14.7-MeV fusion protons at the separator and are guided to collector plates installed at the edge of respective accessible regions. Since the fraction of energy carried by low-energy charged particles is small in an IEC fusion system, the structure of the collector plate can be relatively simple. Because of their large inertia, the 14.7-MeV fusion protons pass through the separator and travel to the modulator. The modulator modifies the velocity of fusion protons to provide bunching downstream. This bunched proton flow excites an alternating electric oscillation on the transmission line that couples to the flow through an array of meshed grids immersed into the flow stream. Studies of meshed grid performance and numerical optimization analyses confirm the reliability of the design for the traveling wave direct energy converter. These studies assumed converters connected to a field-reversed configuration as opposed to an IEC. Nevertheless, the results remain applicable if the power density of proton influx is retained at approximately 10 MW/m^2. A grid array with a radius of 2 m allows conversion of 125 MW of fusion power carried by protons into electricity. These considerations define a representative energy conversion for the IEC. A representative drawing of this system with 250 MW_f of fusion power is shown in Fig.10. The number of IEC modules is arbitrary and the converter could be employed on both wings. For a case of single ended system, a strong magnetic mirror must replace one of the TWDEC. The radius of TWDEC depends on the fusion power handled: 2 m for a 150-MWe system and 5 m for a 1,000-MWe system. The size of IEC module is fixed, being determined mainly by the energy of fusion protons. The length of the direct energy converter is also fixed by the proton energy.

The weight of the conversion system is one of great importance for space propulsion. The weight of an IEC

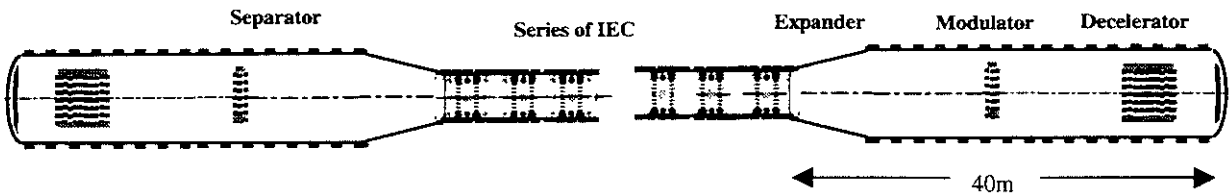

Fig.10: A representative drawing of the system with 250MW of fusion power carried by 14.7MeV protons. Output electricity is 150MWe. For a single ended system, a strong magnetic mirror has to replace one of the TWDEC.

module for D-^{3}He fusion is ~6 tons, and the weight of a pair of direct energy converters is 35 tons for a 250-MW_f system. Thus the total weight is approximately 185 tons provided that a 10-MW_f IEC module is available. The weight normalized by the output power decreases as the fusion power increases. A definite number, however, requires developments on IEC studies yet to be determined.

The present study focuses on conversion of the fusion energy to electricity, which can be used for propulsion and also station keeping. A direct exhaust of protons is possible, but this approach suffers from an unwanted waste of leaking unburned fusion fuel (including helium3). Indeed, the burn fraction of the fuel particles is estimated to be less than a few percent. Since a 250-MW D-^{3}He fusion system consumes 14-kg helium-3 per year, on the order of 1,000-kg a year of helium-3 is wasted. This unwanted loss of expensive helium-3 fuel is avoided in the present conversion system, since all fuel species are contained inside a closed loop. The overall efficiency will, however, decrease to less than 60% in such a conversion system. Further, the associated waste heat, ~100 MW, must be into space. If no steam motor generator is employed in the system, the temperature of the radiation panel can be as high as 600°K. Then a radiation panel of ~ 7000 m^2 would be required for a 250-MW D-^{3}He fusion system with direct energy converter system. This represents additional but acceptable added weight to the system.

In conclusion, the D-^{3}He burning IEC fusion system appears to be attractive in view of the reliable engineering basis for developing the system, the small weight-to-power ratio, the relatively small heat removal system as well as the available recycle leaking unburned fuels. Nevertheless, intensive studies of the IEC fusion core are essential to bring this system to a demonstration stage.

Acknowledgments

This work was carried out as a part of collaborating program of the National Institute for Fusion science. This work was partially supported under a Small Business Innovative Research Contract with NASA's Marshall Space Flight Center, under contract #NAS8-00003.

References

1) R. L. J. Hirsch, Appl. Physics **38** (1969) 4522
2) G. H. Miley, et al., IEEE Trans. On Plasma Science, **25** (1997) 4 , 733-739
3) G. H. Miley and Y. Gu, "*Current Trends in International Fusion Research*", E. Panarella, ed., NRC Press, Canada, 1999, 177-195
4) H. Momota, LA-11808-C, *Los Alamos National Laboratory (1990)* 8-13
5) T. Ishikawa, et al., Fusion Engineering and Design **4** (1998) 541
6) H. Momota, et al., Trans. Fusion Technology **35** (1998) 60
7) T. Takahashi, Y. Tomita, H. Momota, N. V. Shabrov, Plasma Physics 4 (1997) 1-7
8) L.Shu and Y. Tomita, J. Plasma and Fusion Research **72** (1996) 448-452
9) H. Momota, et al., Fusion Technology **21** (1992) 2307-2323

Recent Issues of NIFS Series

NIFS-577 S. Fujiwara and T. Sato,
Molecular Dynamics Simulation of Structure Formation of Short Chain Molecules; Nov 1998

NIFS-578 T. Yamagishi,
Eigenfunctions for Vlasov Equation in Multi-species Plasmas Nov. 1998

NIFS-579 M. Tanaka, A. Yu Grosberg and T. Tanaka,
Molecular Dynamics of Strongly-Coupled Multichain Coulomb Polymers in Pure and Salt Aqueous Solutions; Nov. 1998

NIFS-580 J. Chen, N. Nakajima and M. Okamoto,
Global Mode Analysis of Ideal MHD Modes in a Heliotron/Torsatron System: I. Mercier-unstable Equilibria, Dec 1998

NIFS-581 M. Tanaka, A. Yu Grosberg and T. Tanaka,
Comparison of Multichain Coulomb Polymers in Isolated and Periodic Systems: Molecular Dynamics Study; Jan. 1999

NIFS-582 V.S. Chan and S. Murakami,
Self-Consistent Electric Field Effect on Electron Transport of ECH Plasmas; Feb 1999

NIFS-583 M. Yokoyama, N. Nakajima, M. Okamoto, Y. Nakamura and M. Wakatani,
Roles of Bumpy Field on Collisionless Particle Confinement in Helical-Axis Heliotrons; Feb 1999

NIFS-584 T.-H. Watanabe, T. Hayashi, T. Sato, M. Yamada and H. Ji,
Modeling of Magnetic Island Formation in Magnetic Reconnection Experiment, Feb. 1999

NIFS-585 R. Kumazawa, T. Mutoh, T. Seki, F. Shinpo, G. Nomura, T. Ido, T. Watari, Jean-Marie Noterdaeme and Yangping Zhao,
Liquid Stub Tuner for Ion Cyclotron Heating, Mar. 1999

NIFS-586 A. Sagara, M. Iima, S. Inagaki, N. Inoue, H. Suzuki, K. Tsuzuki, S. Masuzaki, J. Miyazawa, S. Morita, Y. Nakamura, N. Noda, B. Peterson, S. Sakakibara, T. Shimozuma, H. Yamada, K. Akaishi, H. Chikaraishi, H. Funaba, O. Kaneko, K. Kawahata, A. Komori, N. Ohyabu, O. Motojima, LHD Exp. Group 1, LHD Exp. Group 2,
Wall Conditioning at the Starting Phase of LHD, Mar 1999

NIFS-587 T. Nakamura and T. Yabe,
Cubic Interpolated Propagation Scheme for Solving the Hyper-Dimensional Vlasov-Poisson Equation in Phase Space; Mar 1999

NIFS-588 W.X. Wnag, N. Nakajima, S. Murakami and M. Okamoto,
An Accurate δf Method for Neoclassical Transport Calculation; Mar 1999

NIFS-589 K. Kishida, K. Araki, S. Kishiba and K. Suzuki,
Local or Nonlocal? Orthonormal Divergence-free Wavelet Analysis of Nonlinear Interactions in Turbulence, Mar. 1999

NIFS-590 K. Araki, K. Suzuki, K. Kishida and S. Kishiba,
Multiresolution Approximation of the Vector Fields on T^3, Mar. 1999

NIFS-591 K. Yamazaki, H. Yamada, K.Y. Watanabe, K. Nishimura, S. Yamaguchi, H. Nakanishi, A. Komori, H. Suzuki, T. Mito, H. Chikaraishi, K. Murai, O. Motojima and the LHD Group,
Overview of the Large Helical Device (LHD) Control System and Its First Operation; Apr. 1999

NIFS-592 T. Takahashi and Y. Nakao,
Thermonuclear Reactivity of D-T Fusion Plasma with Spin-Polarized Fuel; Apr. 1999

NIFS-593 H. Sugama,
Damping of Toroidal Ion Temperature Gradient Modes; Apr. 1999

NIFS-594 Xiaodong Li,
Analysis of Crowbar Action of High Voltage DC Power Supply in the LHD ICRF System; Apr. 1999

NIFS-595 K. Nishimura, R. Horiuchi and T. Sato,
Drift-kink Instability Induced by Beam Ions in Field-reversed Configurations; Apr 1999

NIFS-596 Y. Suzuki, T-H. Watanabe, T. Sato and T. Hayashi,
Three-dimensional Simulation Study of Compact Toroid Plasmoid Injection into Magnetized Plasmas; Apr. 1999

NIFS-597 H. Sanuki, K. Itoh, M. Yokoyama, A. Fujisawa, K. Ida, S. Toda, S.-I. Itoh, M. Yagi and A. Fukuyama,
Possibility of Internal Transport Barrier Formation and Electric Field Bifurcation in LHD Plasma;
May 1999

NIFS-598 S. Nakazawa, N. Nakajima, M. Okamoto and N. Ohyabu,
One Dimensional Simulation on Stability of Detached Plasma in a Tokamak Divertor; June 1999

NIFS-599 S. Murakami, N. Nakajima, M. Okamoto and J. Nhrenberg,
Effect of Energetic Ion Loss on ICRF Heating Efficiency and Energy Confinement Time in Heliotrons,
June 1999

NIFS-600 R. Horiuchi and T. Sato,
Three-Dimensional Particle Simulation of Plasma Instabilities and Collisionless Reconnection in a Current Sheet;, June 1999

NIFS-601 W. Wang, M. Okamoto, N. Nakajima and S. Murakami,
Collisional Transport in a Plasma with Steep Gradients; June 1999

NIFS-602 T. Mutoh, R. Kumazawa, T. Saki, K. Saito, F. Simpo, G. Nomura, T. Watari, X. Jikang, G. Cattanei, H. Okada, K. Ohkubo, M. Sato, S. Kubo, T. Shimozuma, H. Idei, Y. Yoshimura, O. Kaneko, Y. Takeiri, M. Osakabe, Y. Oka, K. Tsumori, A. Komori, H. Yamada, K. Watanabe, S. Sakakibara, M. Shoji, R. Sakamoto, S. Inagaki, J. Miyazawa, S. Morita, K. Tanaka, B.J. Peterson, S. Murakami, T. Minami, S. Ohdachi, S. Kado, K. Narihara, H. Sasao, H. Suzuki, K. Kawahata, N. Ohyabu, Y. Nakamura, H. Funaba, S. Masuzaki, S. Muto, K. Sato, T. Morisaki, S. Sudo, Y. Nagayama, T. Watanabe, M. Sasao, K. Ida, N. Noda, K. Yamazaki, K. Akaishi, A. Sagara, K. Nishimura, T. Ozaki, K. Toi, O. Motojima, M. Fujiwara, A. Iiyoshi and LHD Exp. Group 1 and 2,
First ICRF Heating Experiment in the Large Helical Device; July 1999

NIFS-603 P.C. de Vries, Y. Nagayama, K. Kawahata, S. Inagaki, H. Sasao and K. Nagasaki,
Polarization of Electron Cyclotron Emission Spectra in LHD; July 1999

NIFS-604 W. Wang, N. Nakajima, M. Okamoto and S. Murakami,
δf Simulation of Ion Neoclassical Transport; July 1999

NIFS-605 T. Hayashi, N. Mizuguchi, T. Sato and the Complexity Simulation Group,
Numerical Simulation of Internal Reconnection Event in Spherical Tokamak, July 1999

NIFS-606 M. Okamoto, N. Nakajima and W. Wang,
On the Two Weighting Scheme for δf Collisional Transport Simulation; Aug. 1999

NIFS-607 O. Motojima, A.A. Shishkin, S. Inagaki, K.Y. Watanabe,
Possible Control Scenario of Radial Electric Field by Loss-Cone-Particle Injection into Helical Device; Aug. 1999

NIFS-608 R. Tanaka, T. Nakamura and T. Yabe,

Constructing Exactly Conservative Scheme in Non-conservative Form, Aug 1999

NIFS-609 H Sugama,
Gyrokinetic Field Theory, Aug 1999

NIFS-610 M Takechi, G Matsunaga, S Takagi, K Ohkuni, K Toi, M Osakabe, M Isobe, S Okamura, K Matsuoka, A Fujisawa, H Iguchi, S Lee, T. Minami, K Tanaka, Y Yoshimura and CHS Group,
Core Localized Toroidal Alfven Eigenmodes Destabilized By Energetic Ions in the CHS Heliotron/Torsatron, Sep 1999

NIFS-611 K Ichiguchi,
MHD Equilibrium and Stability in Heliotron Plasmas, Sep 1999

NIFS-612 Y Sato, M Yokoyama, M Wakatani and V. D. Pusovitov,
Complete Suppression of Pfirsch-Schluter Current in a Toroidal l=3 Stellarator, Oct. 1999

NIFS-613 S. Wang, H. Sanuki and H. Sugama,
Reduced Drift Kinetic Equation for Neoclassical Transport of Helical Plasmas in Ultra-low Collisionality Regime; Oct. 1999

NIFS-614 J. Miyazawa, H. Yamada, K Yasui, S Kato, N., Fukumoto, M Nagata and T. Uyama,
Design of Spheromak Injector Using Conical Accelerator for Large Helical Device; Nov. 1999

NIFS-615 M. Uchida, A Fukuyama, K Itoh, S-I itoh and M. Yagi,
Analysis of Current Diffusive Ballooning Mode in Tokamaks; Dec 1999

NIFS-616 M. Tanaka, A.Yu Grosberg and T. Tanaka,
Condensation and Swelling Behavior of Randomly Charged Multichain Polymers by Molecular Dynamics Simulations; Dec. 1999

NIFS-617 S. Goto and S. Kida,
Sparseness of Nonlinear Coupling; Dec 1999

NIFS-618 M.M. Skoric, T Sato, A Maluckov and M.S Jovanovic,
Complexity in Laser Plasma Instabilities Dec. 1999

NIFS-619 T-H Watanabe, H Sugama and T Sato,
Non-dissipative Kinetic Simulation and Analytical Solution of Three-mode Equations of Ion Temperature Gradient Instability; Dec. 1999

NIFS-620 Y. Oka, Y. Takeiri, Yu.I.Belchenko, M. Hamabe, O. Kaneko, K Tsumori, M. Osakabe, E. Asano, T. Kawamoto, R. Akiyama,
Optimization of Cs Deposition in the 1/3 Scale Hydrogen Negative Ion Source for LHD-NBI System ,Dec. 1999

NIFS-621 Yu.I. Belchenko, Y. Oka, O Kaneko, Y Takeiri, A Krivenko, M. Osakabe, K Tsumori, E Asano, T. Kawamoto, R Akiyama,
Recovery of Cesium in the Hydrogen Negative Ion Sources; Dec. 1999

NIFS-622 Y. Oka, O. Kaneko, K. Tsumori, Y. Takeiri, M. Osakabe, T. Kawamoto, E. Asano, and R. Akiyama,
H- Ion Source Using a Localized Virtual Magnetic Filter in the Plasma Electrode: Type I LV Magnetic Filter: Dec 1999

NIFS-623 M. Tanaka, S Kida, S. Yanase and G. Kawahara,
Zero-absolute-vorticity State in a Rotating Turbulent Shear Flow; Jan. 2000

NIFS-624 F. Leuterer, S. Kubo,
Electron Cyclotron Current Drive at $\omega \approx \omega_c$ with X-mode Launched from the Low Field Side; Feb. 2000

NIFS-625 K. Nishimura,
Wakefield of a Charged Particulate Influenced by Emission Process of Secondary Electrons; Mar. 2000

NIFS-626 K. Itoh, M. Yagi, S.-I. Itoh, A. Fukuyama,
On Turbulent Transport in Burning Plasmas; Mar. 2000

NIFS-627 K. Itoh, S.-I. Itoh, L. Giannone,
Modelling of Density Limit Phenomena in Toroidal Helical Plasmas; Mar. 2000

NIFS-628 K. Akaishi, M. Nakasuga and Y. Funato,
True and Measured Outgassing Rates of a Vacuum Chamber with a Reversibly Absorbed Phase; Mar. 2000

NIFS-629 T. Yamagishi,
Effect of Weak Dissipation on a Drift Orbit Mapping; Mar. 2000

NIFS-630 S. Toda, S.-I, Itoh, M. Yagi, A. Fukuyama and K. Itoh,
Spatial Structure of Compound Dither in L/H Transition; Mar 2000

NIFS-631 N. Ishihara and S. Kida,
Axial and Equatorial Magnetic Dipoles Generated in a Rotating Spherical Shell; Mar. 2000

NIFS-632 T. Kuroda, H. Sugama, R. Kanno and M. Okamoto,
Ion Temperature Gradient Modes in Toroidal Helical Systems; Apr 2000

NIFS-633 V.D. Pustovitov,
Magnetic Diagnostics: General Principles and the Problem of Reconstruction of Plasma Current and Pressure Profiles in Toroidal Systems; Apr. 2000

NIFS-634 A.B. Mikhailovskii, S.V. Konovalov, V.D. Pustovitov and V.S. Tsypin,
Mechanism of Viscosity Effect on Magnetic Island Rotation; Apr. 2000

NIFS-635 H. Naitou, T. Kuramoto, T. Kobayashi, M. Yagi, S. Tokuda and T. Matsumoto,
Stabilization of Kinetic Internal Kink Mode by Ion Diamagnetic Effects; Apr. 2000

NIFS-636 A. Kageyama and S. Kida,
A Spectral Method in Spherical Coordinates with Coordinate Singularity at the Origin, Apr. 2000

NIFS-637 R. Horiuchi, W. Pei and T. Sato,
Collisionless Driven Reconnection in an Open System; June 2000

NIFS-638 K. Nagaoka, A. Okamoto, S. Yoshimura and M.Y. Tanaka,
Plasma Flow Measurement Using Directional Langmuir Probe under Weakly Ion-Magnetized Conditions; July 2000

NIFS-639 Alexei Ivanov,
Scaling of the Distribution Function and the Critical Exponents near the Point of a Marginal Stability under the Vlasov-Poisson Equations; Aug 2000

NIFS-640 K. Ohi, H. Naitou, Y. Tauchi, O. Fukumasa,
Observation of the Limit Cycle in the Asymmetric Plasma Divided by the Magnetic Filter; Aug. 2000

NIFS-641 H. Momota, G.H. Miley and J. Nadler,
Direct Energy Conversion for IEC Propulsions; Aug. 2000